MODELLING THE DOUBLE CANTILEVER BEAM TEST WITH BENDING MOMENTS BY USING BILINEAR DISCONTINUOUS COHESIVE LAWS

Paolo S. Valvo[1], Bent F. Sørensen[2] and Helmuth L. Toftegaard[2]

[1]Department of Department of Civil and Industrial Engineering, University of Pisa
Largo Lucio Lazzarino, I-56122 Pisa, Italy
Email: p.valvo@ing.unipi.it, web page: http://www.unipi.it

[2]Department of Wind Energy, Technical University of Denmark
Frederiksborgvej 399, DK-4000 Roskilde, Denmark
Email: bsqr@dtu.dk, heto@dtu.dk, web page: http://www.dtu.dk

Keywords: Composite delamination, Cohesive law, Double cantilever beam test, Analytical solution, Experimental testing

ABSTRACT

A theoretical model of the double cantilever beam tests with bending moments (DCB-UBM) is presented. The specimen is modelled as the assemblage of two laminated beams connected by a cohesive interface. It is assumed that the traction-separation laws – *i.e.* the relationships between the interfacial stresses and relative displacements – are described by bilinear discontinuous functions. An analytical solution for pure modes I and II is determined by solving the related differential problem. Furthermore, analysis based on the path-independent *J* integral is carried out. Formulas are given to determine the cohesive law parameters from experiments. Experimental tests have been conducted on glass fibre reinforced specimens under pure mode I and II loading conditions. The predictions of the theoretical model turn out to be in very good agreement with the experimental results.

1 INTRODUCTION

The double cantilever beam test with bending moments (DCB-UBM) is a test used to characterise the delamination toughness of fibre-reinforced composite laminates [1]. In comparison with the standard DCB test, where the specimen is loaded with forces [2], the DCB-UBM test has several advantages. Depending on the ratio between the applied moments, the whole range of crack opening displacements (from pure normal to pure tangential) can be obtained. Furthermore, crack propagation is always stable. Lastly, test results are independent of crack length and shear modulus.

The DCB-UBM test can be modelled by using simple beam theory, which is however unable to describe the deformation at the fracture process zone. A model where the delaminating arms of the specimen are connected by an elastic interface [3] gives good prediction of the specimen's response prior to crack propagation, but is unsatisfactory to describe the crack growth stage (in particular, under large-scale bridging). In this case, it is more appropriate to use cohesive laws, which furnish the local normal and shear stresses as functions of the corresponding relative displacements [4].

We have conducted experimental tests on glass fibre-reinforced specimens loaded under pure normal and near pure tangential crack opening displacements. Then, we have tried to reproduce the experimental results via a theoretical model, where the specimens is modelled as the assemblage of two laminated beams connected by a cohesive interface. We have tested many possible shapes for the cohesive laws (bilinear, rectangular, exponential, etc.). After some trial and error, we have ended up with the proposal of using bilinear discontinuous cohesive laws. Then, we have deduced an analytical solution for the differential problem that describes the model under pure modes I and II. Furthermore, we have carried out an analysis based on the path-independent *J* integral. The cohesive law parameters can be determined from the experimental results by means of practical formulas. The predictions of the theoretical model agree very well with the experimental results for the whole response of the specimen, from the initial linearly elastic stage to crack initiation and steady-state crack propagation.

2 THEORETICAL MODEL

2.1 Specimen

Fig. 1 shows a schematic of the double cantilever beam test with bending moments. The specimen is a laminated beam of length L, thickness $H = 2\,h$ and width B (not shown in the figure). A mid-plane delamination of length a is present at one end. We assume that the specimen has a symmetric (but not necessarily unidirectional) stacking sequence. Two independent bending moments, M_1 and M_2, are applied at the delaminated end of the specimen. The undelaminated end is restricted from rotation, but can move freely in the longitudinal direction. To describe our model, we fix a reference system Oxz with the origin at the delamination crack tip and the x- and z-axes respectively aligned with the specimen's longitudinal and transverse directions.

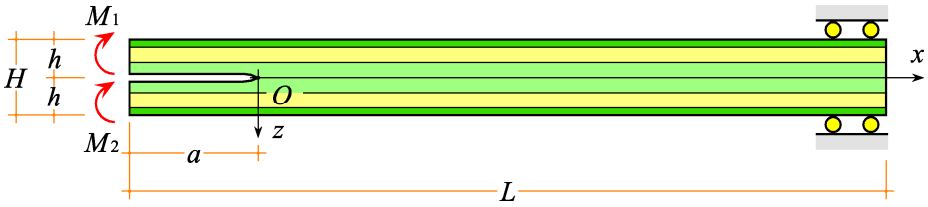

Figure 1: The double cantilever beam test with bending moments.

The applied bending moments can be split into the sum of two symmetric moments $M_s = (M_1 + M_2) / 2$ and two antisymmetric moments $M_a = (M_1 - M_2) / 2$ (Fig. 2). In line with Linear Elastic Fracture Mechanics (LEFM), given the symmetry of the specimen with respect to its mid-plane, the symmetric and antisymmetric load conditions respectively correspond to mode I (opening) and mode II (sliding) crack propagation. The adopted experimental setup enables to fix the ratio between the applied moments, M_1 / M_2, to obtain different values of mode mixity [1].

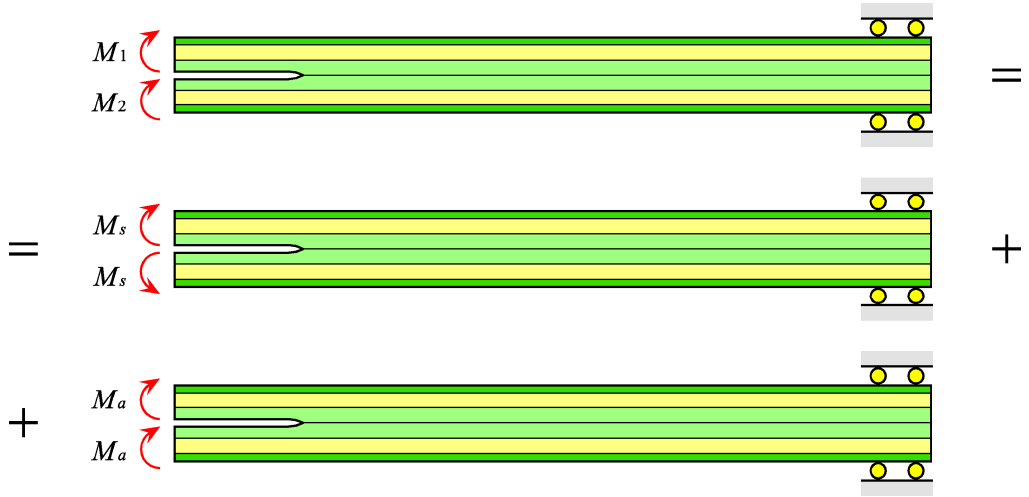

Figure 2: Mode I and II load conditions.

The specimen is modelled as the assemblage of two laminated beams – the upper and lower sublaminates, respectively denoted as No. 1 and 2 – connected by a cohesive interface, which transfers normal and shear stresses, σ and τ (Fig. 3). We denote with u_α and w_α respectively the *axial* and *transverse displacements* of the sublaminates' centrelines and with ϕ_α their *cross sections' rotations*. Here and in the following, the subscript $\alpha \in \{1, 2\}$ refers to the sublaminate number. According to Timoshenko's beam theory, we define the *axial strain*, *shear strain*, and *curvature* respectively as

$$\varepsilon_\alpha = \frac{du_\alpha}{dx}, \quad \gamma_\alpha = \frac{dw_\alpha}{dx} + \phi_\alpha, \quad \text{and} \quad \kappa_\alpha = \frac{d\phi_\alpha}{dx}. \tag{1}$$

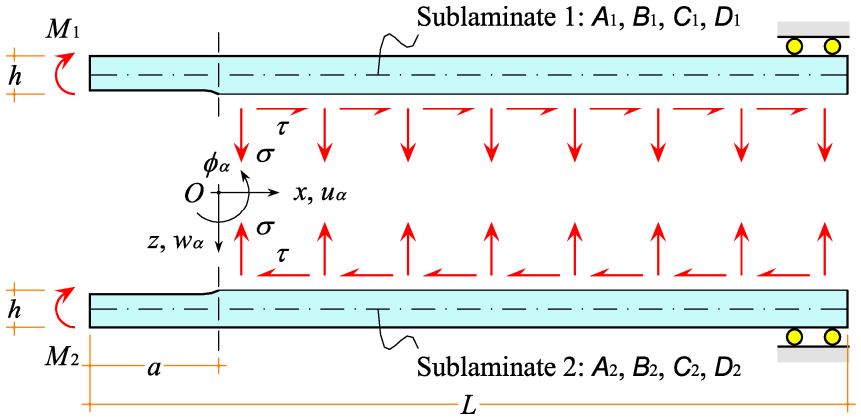

Figure 3: Mechanical model.

According to classical lamination theory [7], we denote with A_1, B_1, C_1, and D_1 respectively the *extensional stiffness*, *bending-extension coupling stiffness*, *shear stiffness*, and *bending stiffness* per unit width of the upper sublaminate. For homogeneous isotropic and unidirectional specimens, $A_1 = E_x\, h$, $B_1 = 0$, $C_1 = 5\, G_{zx}\, h / 6$, and $D_1 = E_x\, h^3 / 12$, where E_x and G_{zx} respectively are the Young's modulus and shear modulus of the material in the *xz*-plane. Because of the assumed symmetry of the specimen, the stiffnesses of the lower sublaminate are $A_2 = A_1$, $B_2 = -B_1$, $C_2 = C_1$, and $D_2 = D_1$.

To simplify subsequent calculations, we also define the *compliances*,

$$a_\alpha = \frac{D_\alpha}{A_\alpha D_\alpha - B_\alpha^2}, \quad b_\alpha = -\frac{B_\alpha}{A_\alpha D_\alpha - B_\alpha^2}, \quad c_\alpha = \frac{1}{C_\alpha}, \quad \text{and} \quad d_\alpha = \frac{A_\alpha}{A_\alpha D_\alpha - B_\alpha^2}. \tag{2}$$

The *axial force*, *shear force*, and *bending moment* in the sublaminates respectively are

$$N_\alpha = B\left(A_\alpha \varepsilon_\alpha + B_\alpha \kappa_\alpha\right), \quad Q_\alpha = B\, C_\alpha \gamma_\alpha, \quad \text{and} \quad M_\alpha = B\left(B_\alpha \varepsilon_\alpha + D_\alpha \kappa_\alpha\right). \tag{3}$$

Considering the sign convention for the distributed loads, the equilibrium equations for the two sublaminates turn out to be the following:

$$\frac{dN_\alpha}{dx} - (-1)^\alpha\, B\tau = 0, \quad \frac{dQ_\alpha}{dx} - (-1)^\alpha\, B\sigma = 0, \quad \text{and} \quad \frac{dM_\alpha}{dx} + \frac{1}{2} Bh\tau - Q_\alpha = 0. \tag{4}$$

2.2 Cohesive laws

Cohesive zone models assume that the interfacial stresses are functions of the relative displacements between the corresponding points on the separating crack faces. In particular, we define the *sliding* (tangential) and *opening* (normal) *displacements* respectively as

$$\Delta u = u_2 - u_1 - \frac{h}{2}\left(\phi_1 + \phi_2\right) \quad \text{and} \quad \Delta w = w_2 - w_1. \tag{5}$$

Under mixed-mode loading conditions, the normal stress, σ, and shear stress, τ, are functions of both Δu and Δw. However, under pure mode I, because of the symmetry conditions, $\Delta u = 0$ and $\tau = 0$. Likewise, under pure mode II, $\Delta w = 0$ and $\sigma = 0$. In such cases, σ is a function of Δw alone and τ is a function of Δu alone [5]. Here, we assume the following piecewise linear traction-separation laws:

$$\sigma(\Delta w) = \begin{cases} \sigma_0 \dfrac{\Delta w}{\Delta w_0}, & \text{if} \quad 0 \le \Delta w < \Delta w_0; \\ \sigma_1 \dfrac{\Delta w_u - \Delta w}{\Delta w_u - \Delta w_0}, & \text{if} \quad \Delta w_0 \le \Delta w < \Delta w_u; \\ 0, & \text{if} \quad \Delta w_u \le \Delta w; \end{cases} \tag{6}$$

and

$$\tau(\Delta u) = \begin{cases} \tau_0 \dfrac{\Delta u}{\Delta u_0}, & \text{if} \quad 0 \le \Delta u < \Delta u_0; \\ \tau_1, & \text{if} \quad \Delta u_0 \le \Delta u. \end{cases} \tag{7}$$

Eq. (6) holds for the pure mode I loading condition. In this case, the traction-separation law has an initial linear branch where the normal stress, σ, increases from zero to a maximum value, σ_0, while the opening displacement, Δw, goes from zero to Δw_0. A discontinuous linear branch follows, where the normal stress decreases from σ_1 to zero, while the opening displacement goes from Δw_0 to Δw_u. The normal stress is zero for all the values of Δw greater than Δw_u (Fig. 4a). On the other hand, Eq. (7) holds for the pure mode II loading condition. In this case, the traction-separation law has an initial linear branch where the shear stress, τ, increases from zero to a maximum value, τ_0, while the sliding displacement, Δu, goes from zero to Δu_0. A discontinuous horizontal branch follows, where the shear stress has the constant value τ_1 (Fig. 4b). For both the normal and shear stresses, the initial linear branches represent initial stages, where the material behaves elastically. The subsequent discontinuous branches represent progressive damage of the material. For mode I, fracture occurs when $\Delta w \ge \Delta w_u$. For mode II, such a definite limit for fracture is not considered. This is consistent with previous findings about mode II delamination [6].

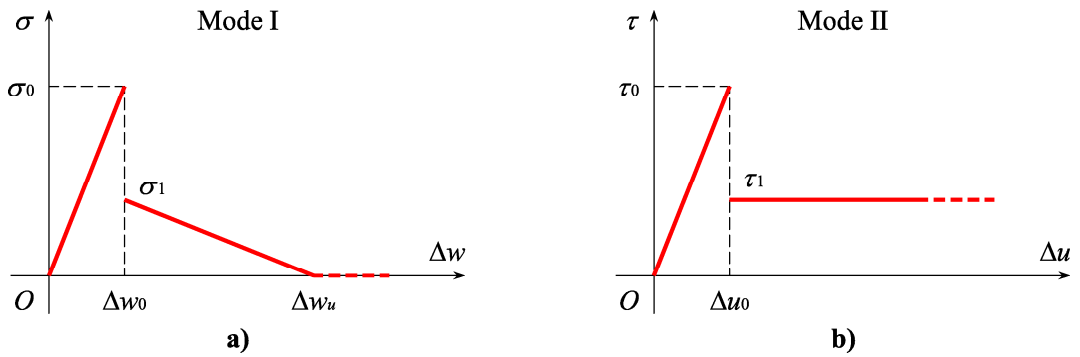

Figure 4: Traction-separation laws: a) normal stress vs. opening displacement; b) shear stress vs. sliding displacement.

2.3 Solution for mode I

The mechanical model based on the aforesaid assumptions can be mathematically described by a system of differential equations and boundary conditions. To this aim, Eqs. (1)–(7) are suitably combined to obtain differential equations for the normal and shear interfacial stresses, which play the role of principal unknowns. Then, an analytical solution has been determined for the cases of pure modes I and II. Here, for the sake of brevity, we present only the main results and postpone a detailed description of the mathematical derivation to a forthcoming extended paper.

Under pure mode I loading, thanks to the symmetry conditions, the analysis can be limited to the upper half of the specimen (Fig. 5). During the test, under increasing load, the opening displacements in the cohesive zone increase monotonically and attain their maximum at the crack-tip cross section. Three stages can be individualised in the specimen's response:

- *Stage I – Linearly elastic behaviour*. As long as the opening displacement at the crack tip, $\Delta w(0)$, is less than Δw_0, the specimen's response is linearly elastic. Neither material damage, nor crack propagation occur during this stage;
- *Stage II – Progressive material damage*. When the opening displacement at the crack tip attains the value Δw_0, damage of the material begins. As the test proceeds further, a damaged zone of increasing length, d, develops ahead of the crack tip. Correspondingly, the length, e, of the zone where the material is still linearly elastic decreases;

- *Stage III – Crack propagation.* When the opening displacement at the crack tip equals Δw_u, fracture occurs. Then, the process goes on with the delamination length, a, that increases and the damaged zone that moves along the specimen's longitudinal direction. In practice, real specimens are so long that we can simplify the modelling by assuming $L \to \infty$. In this case, after the crack begins to propagate, it will continue propagating under steady state conditions.

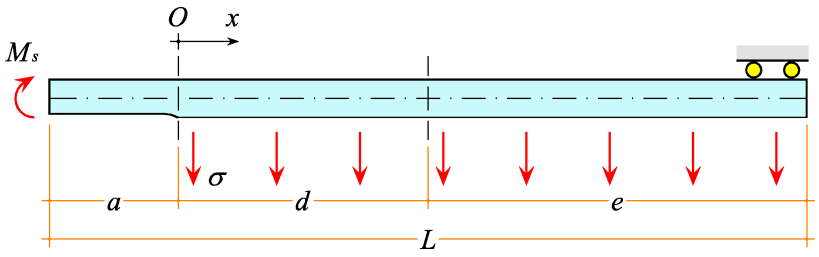

Figure 5: Upper half of the specimen under mode I loading.

The normal interfacial stress turns out to have the following expression:

$$\sigma(x) = \begin{cases} G_1 \cos(\mu_1 x) + G_2 \sin(\mu_1 x) + G_3 \cosh(\mu_2 x) + G_4 \sinh(\mu_2 x), & \text{if} \quad 0 \le x < d; \\ F_1 \exp[-\lambda_1 (x-d)] + F_2 \exp[-\lambda_2 (x-d)], & \text{if} \quad d \le x; \end{cases} \tag{8}$$

where λ_1, λ_2, μ_1, and μ_2 are roots of the characteristic equations for σ. Their expressions are given in the appendix. Besides, F_1, F_2, G_1, G_2, G_3, and G_4 are integration constants, which are determined by solving the following equation set, representing the boundary conditions at $x = 0$ and $x = d$:

$$\begin{cases} F_1 + F_2 = \sigma_0; \\ \dfrac{F_1}{\lambda_1} + \dfrac{F_2}{\lambda_2} + G_1 \dfrac{\sin(\mu_1 d)}{\mu_1} - G_2 \dfrac{\cos(\mu_1 d)}{\mu_1} + G_3 \dfrac{\sinh(\mu_2 d)}{\mu_2} + G_4 \dfrac{\cosh(\mu_2 d)}{\mu_2} = 0; \\ \dfrac{F_1}{\lambda_1^2} + \dfrac{F_2}{\lambda_2^2} + G_1 \dfrac{\cos(\mu_1 d)}{\mu_1^2} + G_2 \dfrac{\sin(\mu_1 d)}{\mu_1^2} - G_3 \dfrac{\cosh(\mu_2 d)}{\mu_2^2} - G_4 \dfrac{\sinh(\mu_2 d)}{\mu_2^2} = 0; \\ \dfrac{F_1}{\lambda_1^3} + \dfrac{F_2}{\lambda_2^3} - G_1 \dfrac{\sin(\mu_1 d)}{\mu_1^3} + G_2 \dfrac{\cos(\mu_1 d)}{\mu_1^3} + G_3 \dfrac{\sinh(\mu_2 d)}{\mu_2^3} + G_4 \dfrac{\cosh(\mu_2 d)}{\mu_2^3} = 0; \\ G_1 \cos(\mu_1 d) + G_2 \sin(\mu_1 d) + G_3 \cosh(\mu_2 d) + G_4 \sinh(\mu_2 d) = \sigma_1; \\ \dfrac{G_2}{\mu_1} - \dfrac{G_4}{\mu_2} = 0; \\ \dfrac{G_1}{\mu_1^2} - \dfrac{G_3}{\mu_2^2} = \dfrac{M_s}{B}. \end{cases} \tag{9}$$

Eqs. (9) contain seven equations, but there are only six unknown integration constants. Actually, an additional unknown is the length of the damaged zone, d (or, alternatively, the applied bending moment, M_s). In this regard, we note that during stage I, d is zero. During stage II, d varies between zero and a maximum value, d_u. During stage III, under steady-state crack propagation, d is constant and equal to d_u. In this case, Eq. (8) still describes the normal stress distribution, provided that the origin O is suitably moved along the specimen to coincide with the new positions of the crack tip.

By substituting $d = 0$ into Eqs. (9), we calculate the applied bending moment at the end of stage I,

$$M_s^0 = B\sqrt{\frac{\sigma_0 \Delta w_0}{2d_1}}. \tag{10}$$

Furthermore, by adding the condition that $\Delta w = \Delta w_u$ at the crack tip, from Eqs. (9) we determine the equation for d_u:

$$\gamma_{cc}\cos(\mu_1 d_u)\cosh(\mu_2 d_u)+\gamma_{cs}\cos(\mu_1 d_u)\sinh(\mu_2 d_u)+\gamma_{sc}\sin(\mu_1 d_u)\cosh(\mu_2 d_u)+ \\ +\gamma_{ss}\sin(\mu_1 d_u)\sinh(\mu_2 d_u)+\gamma_0=0, \tag{11}$$

where the coefficients γ_{cc}, γ_{cs}, γ_{sc}, γ_{ss}, and γ_0 have lengthy expressions, that are omitted here for the sake of brevity. Eq. (11) can be solved numerically to obtain d_u as its smallest positive root. The specimen's response during stage II can then be obtained by letting d vary between 0 and d_u. For each value of the length of the damaged zone, Eqs. (9) can be solved to get M_s. For $d = d_u$, the constant bending moment of stage III, M_s^u, is obtained. Alternatively, as will explained in the following, the specimen's response can be obtained more simply by using the path-independent J integral.

2.4 Solution for mode II

Under pure mode II loading, the specimen is subjected to antisymmetric loads with respect to its mid-plane. As for the pure mode I case, the analysis can be limited to the upper half of the specimen (Fig. 6). During the test, under increasing load, the sliding displacements in the cohesive zone increase monotonically and attain their maximum at the crack-tip cross section. Two stages can be individualised in the specimen's response:

- *Stage I – Linearly elastic behaviour*. As long as the sliding displacement at the crack tip, $\Delta u(0)$, is less than Δu_0, the specimen's response is linearly elastic. Neither material damage, nor crack propagation occur during this stage;
- *Stage II – Progressive material damage*. When the sliding displacement at the crack tip attains the value Δu_0, damage of the material begins. As the test proceeds further, a damaged zone of increasing length, d, develops ahead of the crack tip. Correspondingly, the length, e, of the zone where the material is still linearly elastic decreases.

As a difference with the mode I case, the assumed cohesive law for pure mode II, Eq. (7), does not have a definite limit for material fracture. Therefore, the theoretical model does not predict a crack propagation stage for this loading case.

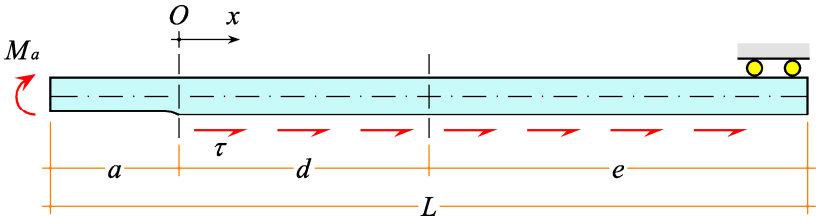

Figure 6: Upper half of the specimen under mode II loading.

The shear interfacial stress turns out to have the following expression:

$$\tau(x)=\begin{cases}\tau_1, & \text{if} \quad 0\le x<d;\\ F_5\exp[-\lambda_5(x-d)], & \text{if} \quad d\le x;\end{cases} \tag{12}$$

where λ_5 is a root of the characteristic equation for τ, whose expression is given in the appendix, and

$$F_5=2\frac{2b_1+d_1h}{4a_1+4b_1h+d_1h^2}\lambda_5\frac{M_a}{B}-\lambda_5\tau_1 d \tag{13}$$

is an integration constant, determined by imposing the boundary conditions at $x = 0$ and $x = d$.

In Eqs. (12) and (13), it must be considered that during stage I, $d = 0$. In this case, by imposing $\tau(0) = \tau_0$ and solving for M_a, we obtain the value of the applied bending moment at the end of stage I,

$$M_a^0=\frac{B}{2\lambda_5}\frac{4a_1+4b_1h+d_1h^2}{2b_1+d_1h}\tau_0. \tag{14}$$

During stage II, by imposing $\tau(d) = \tau_0$ and solving for M_a, we obtain

$$M_a = \frac{B}{2\lambda_5}\frac{4a_1 + 4b_1 h + d_1 h^2}{2b_1 + d_1 h}\left(\tau_0 + \lambda_5 \tau_1 d\right). \tag{15}$$

According to Eq. (15), the applied bending moment should increase unboundedly as the length of the damaged zone, d, increases. In practice, a limit will be given by the finite length of the specimen.

2.5 *J* integral analysis

Besides directly solving the differential problem, as explained in the previous sections, the proposed mechanical model can be analysed by using the path-independent integral [1, 8],

$$J = \oint_\Gamma \left[\omega\, dz - \left(t_x \frac{\partial u}{\partial x} + t_z \frac{\partial w}{\partial x} \right) d\Gamma \right], \tag{16}$$

where ω is the strain energy density, t_x and t_z are the components of the stress vector acting on the path element $d\Gamma$, and Γ is an arbitrary contour encircling the crack tip. As proposed in [5], we consider an external contour, Γ_{ext}, and an internal or local contour, Γ_{loc}, surrounding the cohesive interface (Fig. 7).

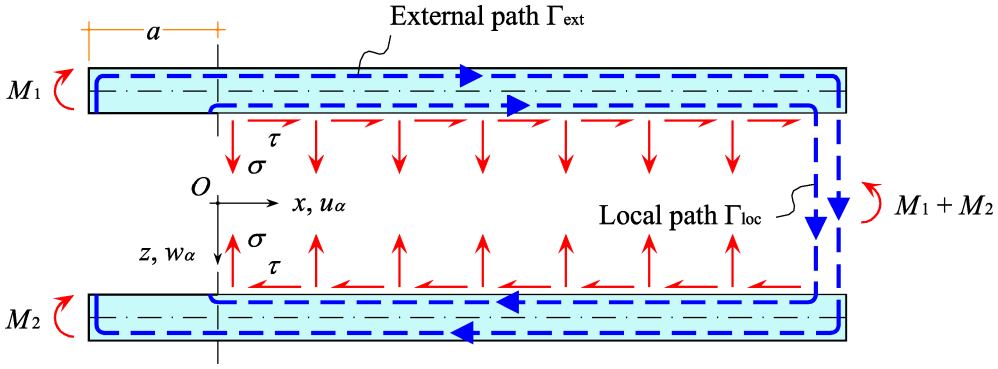

Figure 7: *J* integral analysis.

Evaluation of the *J* integral along the external contour gives

$$J_{\text{ext}} = \frac{d_1\left(M_1^2 + M_2^2\right) - 2\dfrac{a_1 d_1 - b_1^2}{4a_1 + 4b_1 h + d_1 h^2}\left(M_1 + M_2\right)^2}{2B^2}, \tag{17}$$

which under pure mode I and II loadings respectively becomes

$$J_{\text{I}}^{\text{ext}} = d_1 \frac{M_s^2}{B^2} \quad \text{and} \quad J_{\text{II}}^{\text{ext}} = \frac{4b_1^2 + 4b_1 d_1 h + d_1^2 h^2}{4a_1 + 4b_1 h + d_1 h^2}\frac{M_a^2}{B^2}. \tag{18}$$

On the other hand, evaluation of the *J* integral along the internal contour gives

$$J_{\text{I}}^{\text{loc}} = \int_0^{\Delta w(0)} \sigma(\Delta w)\, d\Delta w \quad \text{and} \quad J_{\text{II}}^{\text{loc}} = \int_0^{\Delta u(0)} \tau(\Delta u)\, d\Delta u. \tag{19}$$

Because of the path independence, the quantities computed via Eqs. (18) and (19) must coincide. Hence, we obtain relationships between the values of the opening and sliding displacements at the crack tip, $\Delta w(0)$ and $\Delta u(0)$, and the applied bending moments,

$$M_s = \frac{B}{\sqrt{d_1}}\sqrt{\int_0^{\Delta w(0)} \sigma(\Delta w)\, d\Delta w} \quad \text{and} \quad M_a = B\frac{\sqrt{4a_1 + 4b_1 h + d_1 h^2}}{2b_1 + d_1 h}\sqrt{\int_0^{\Delta u(0)} \tau(\Delta u)\, d\Delta u}. \tag{20}$$

We note that Eqs. (20) hold in general, regardless of the specific cohesive laws that are adopted. But, if we substitute the presently assumed cohesive laws, Eqs. (6) and (7), into (20), we can explicitly write the load-displacement relationships for mode I,

$$M_s = \begin{cases} \dfrac{B}{\sqrt{d_1}}\sqrt{\dfrac{\sigma_0}{2\Delta w_0}}\,\Delta w(0), & \text{if } 0 \le \Delta w(0) < \Delta w_0; \\ \dfrac{B}{\sqrt{d_1}}\sqrt{\dfrac{\sigma_0\Delta w_0}{2}+\dfrac{\sigma_1}{2}\dfrac{\Delta w(0)-\Delta w_0}{\Delta w_u-\Delta w_0}\left[2\Delta w_u-\Delta w(0)-\Delta w_0\right]}, & \text{if } \Delta w_0 \le \Delta w(0) < \Delta w_u; \\ \dfrac{B}{\sqrt{d_1}}\sqrt{\dfrac{\sigma_0\Delta w_0}{2}+\dfrac{\sigma_1}{2}\left(\Delta w_u-\Delta w_0\right)}, & \text{if } \Delta w_u \le \Delta w(0); \end{cases} \tag{21}$$

and mode II,

$$M_a = \begin{cases} B\dfrac{\sqrt{4a_1+4b_1h+d_1h^2}}{2b_1+d_1h}\sqrt{\dfrac{\tau_0}{2\Delta u_0}}\,\Delta u(0), & \text{if } 0 \le \Delta u(0) < \Delta u_0; \\ B\dfrac{\sqrt{4a_1+4b_1h+d_1h^2}}{2b_1+d_1h}\sqrt{\dfrac{\tau_0\Delta u_0}{2}+\tau_1\left[\Delta u(0)-\Delta u_0\right]}, & \text{if } \Delta u_0 \le \Delta u(0). \end{cases} \tag{22}$$

By substituting $\Delta w(0) = \Delta w_0$ and $\Delta u(0) = \Delta u_0$ into Eqs. (21) and (22), respectively, the values of the applied bending moment at the end of the linearly elastic stages are obtained,

$$M_s^0 = \frac{B}{\sqrt{d_1}}\sqrt{\frac{\sigma_0\Delta w_0}{2}} \quad \text{and} \quad M_a^0 = B\frac{\sqrt{4a_1+4b_1h+d_1h^2}}{2b_1+d_1h}\sqrt{\frac{\tau_0\Delta u_0}{2}}, \tag{23}$$

which coincide with the values given by Eqs. (10) and (14), respectively. For homogeneous isotropic and unidirectional laminated specimens, Eqs. (23) simplify to

$$M_s^0 = B\sqrt{\frac{E_x h^3}{12}}\sqrt{\frac{\sigma_0\Delta w_0}{2}} \quad \text{and} \quad M_a^0 = B\sqrt{\frac{E_x h^3}{9}}\sqrt{\frac{\tau_0\Delta u_0}{2}}. \tag{24}$$

Lastly, we note that the value of M_s given by Eq. (21) for $\Delta w(0) \ge \Delta w_u$ is that corresponding to the steady state crack propagation stage, M_s^u.

3 EXPERIMENTAL TESTS

DCB-UBM tests [1] were performed on glass fibre reinforced, unidirectional laminated specimens. The thickness of the specimens was approximately 19 mm, the width was approximately 30 mm. A mid-plane delamination was initiated by a 12.5 μm thick slip foil (70 mm long) placed at the loaded end of the specimen. The elastic moduli have been determined as follows: E_x = 41.2 GPa, E_z = 12.8 GPa, and G_{zx} = 4.6 GPa. The tests were conducted at a displacement rate of 10 mm/min for the lower beam of the test machine [5], and the load was measured by two load cells.

A single mode I test was performed on a specimen of 330 mm length. The moments were applied as forces acting on transverse arms attached to the end of the specimen with moment arms 86.5 mm on both arms (moment ratio $M_1 / M_2 = -1$). The normal opening was measured with an extensometer.

Two tests were performed on 500 mm long specimens in a mode mixity close to mode II (pure mode II would give too much friction between the sublaminates). Moment arms of 161.5 mm and 156.5 mm were used (moment ratio $M_1 / M_2 = 0.97$). The normal opening was measured with an extensometer, and the sliding opening was measured with two LVDTs (linear variable displacement transducers).

4 RESULTS AND DISCUSSION

4.1 Determination of the cohesive law parameters

In order to use the theoretical model to reproduce the experimental results, the parameters that define the cohesive laws, Eqs. (6) and (7), have to be determined. This can be done partly based on theoretical considerations, partly by using some experimental results from the tests themselves.

The initial linear branches of the traction-separation laws correspond to the response of a linear elastic interface,

$$\sigma = k_z \Delta w \quad \text{and} \quad \tau = k_x \Delta u, \tag{25}$$

where k_z and k_x are the elastic constants of a continuous distribution of normal and tangential springs, respectively. Based on energy equivalence [9], the values of the elastic constants can be determined as

$$k_z = \frac{35}{13}\frac{E_z}{2h} \quad \text{and} \quad k_x = \frac{15}{2}\frac{G_{zx}}{2h}, \tag{26}$$

where E_z is the Young's modulus of the material in the transverse direction.

By substituting Eqs. (25) into (24) and solving with respect to the displacements, we obtain

$$\Delta w_0 = \frac{2M_s^0}{B}\sqrt{\frac{6}{k_z E_x h^3}} \quad \text{and} \quad \Delta u_0 = \frac{3M_a^0}{B}\sqrt{\frac{2}{k_x E_x h^3}}. \tag{27}$$

Once M_s^0 and M_a^0 are determined from the experimental tests, Eqs. (27) yield the crack-tip opening and sliding displacements at the end of the linearly elastic stage. Then, Eqs. (25) furnish the corresponding normal and shear stresses, σ_0 and τ_0.

The experimental tests for mode I also furnish the values of displacement, Δw_u, and bending moment, M_s^u, at the beginning of the steady state crack propagation stage. Then, the normal stress σ_1 is obtained by inverting the last expression in Eq. (21). For homogeneous isotropic and unidirectional laminated specimens, we obtain

$$\sigma_1 = \frac{\dfrac{24}{E_x h^3}\left(\dfrac{M_s^u}{B}\right)^2 - \sigma_0 \Delta w_0}{\Delta w_u - \Delta w_0}. \tag{28}$$

For the mode II tests, from the experiments the maximum applied load, M_a^u, and the corresponding sliding displacement, Δu_u, can be determined. Such values are inserted into Eq. (22), which is then solved for the stress τ_1. For homogeneous isotropic and unidirectional laminated specimens, we obtain

$$\tau_1 = \frac{\dfrac{9}{E_x h^3}\left(\dfrac{M_a^u}{B}\right)^2 - \dfrac{\tau_0 \Delta u_0}{2}}{\Delta u_u - \Delta u_0}. \tag{29}$$

From the performed experimental tests, the values listed in Table 1 were determined.

Mode I tests		Mode II tests	
M_s^0	22.0 Nm	M_a^0	80.0 Nm
M_s^u	40.0 Nm	M_a^u	140.0 Nm
Δw_u	1.1 mm	Δu_u	3.5 mm

Table 1: Quantities determined from experimental tests.

Then, by using Eqs. (25)–(29) the quantities listed in Table 2 were calculated.

Mode I tests		Mode II tests	
k_z	1813.8 N/mm^3	k_x	1815.8 N/mm^3
Δw_0	0.014 mm	Δu_0	0.045 mm
σ_0	25.7 MPa	τ_0	81.1 MPa
σ_1	0.8 MPa	τ_1	1.1 MPa

Table 2: Quantities calculated via the theoretical model.

4.2 Experimental results and theoretical predictions

Figure 8a shows the trend of the applied bending moment, M_s, vs. the crack opening displacement, Δw, for the mode I test. Likewise, figure 8b shows the trend of the applied bending moment, M_a, vs. the crack sliding displacement, Δu, for the mode II tests.

The green curves represent the experimental results, while the red curves correspond to the theoretical predictions of the developed model. For both modes I and II, a very good agreement is obtained between the experimental results and theoretical predictions.

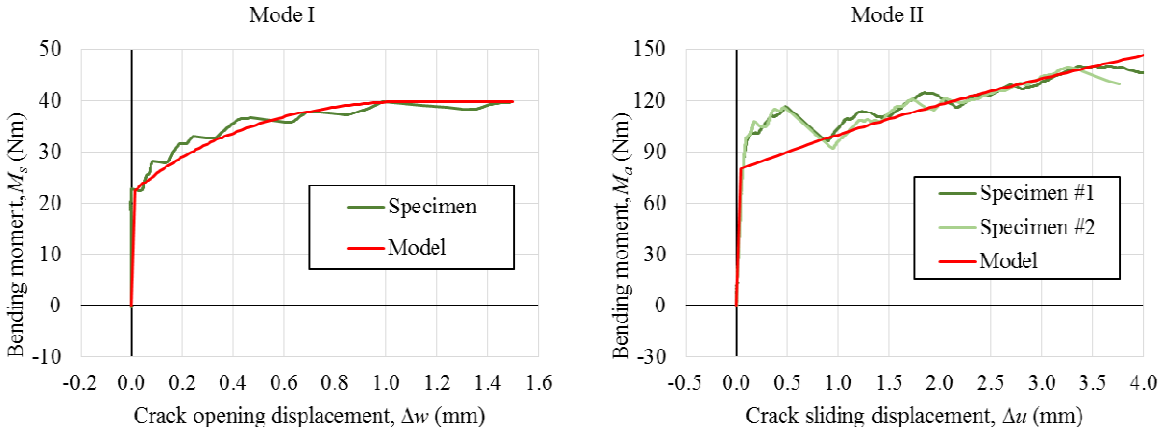

a) **b)**

Figure 8: Applied bending moment vs. crack opening: a) mode I test; b) mode II test.

5 CONCLUSIONS

A theoretical model of the double cantilever beam tests with bending moments (DCB-UBM) has been presented. The model is based on the assumption of bilinear discontinuous cohesive laws. An analytical solution has been determined and practical formulas for the cohesive law parameters have been given. Experimental tests have been conducted on glass fibre reinforced specimens under pure mode I and II loading conditions. The predictions of the theoretical model turn out to be in very good agreement with the experimental results.

Future work involves the development of an analytical solution for mixed mode I/II loading conditions. Actually, this solution cannot be obtained simply by superposition of the solutions for modes I and II because of the nonlinear material behaviour.

ACKNOWLEDGEMENTS

This paper was prepared during the first author's (P.S. Valvo) sabbatical leave at the Technical University of Denmark, DTU Wind Energy, Composite Materials Section (Sept. 2014 – Feb. 2015). Acknowledgements go to all the staff of the Section for their hospitality, support, and scientific advice.

APPENDIX

The roots of the characteristic equations have the following expressions:

$$\lambda_1 = \sqrt{\frac{\sigma_0}{\Delta w_0}\left(c_1 + \sqrt{c_1^2 - 2d_1\frac{\Delta w_0}{\sigma_0}}\right)}, \quad \lambda_2 = \sqrt{\frac{\sigma_0}{\Delta w_0}\left(c_1 - \sqrt{c_1^2 - 2d_1\frac{\Delta w_0}{\sigma_0}}\right)},$$
$$\lambda_5 = \sqrt{\frac{\tau_0}{\Delta u_0}\left(2a_1 + 2b_1 h + \frac{1}{2}d_1 h^2\right)}; \tag{A1}$$

and

$$\mu_1 = \sqrt{\frac{\sigma_1}{\Delta w_u - \Delta w_0}\left(c_1 + \sqrt{c_1^2 + 2d_1\frac{\Delta w_u - \Delta w_0}{\sigma_1}}\right)},$$
$$\mu_2 = \sqrt{\frac{\sigma_1}{\Delta w_u - \Delta w_0}\left(-c_1 + \sqrt{c_1^2 + 2d_1\frac{\Delta w_u - \Delta w_0}{\sigma_1}}\right)}. \tag{A2}$$

REFERENCES

[1] B.F. Sørensen, K. Jørgensen, T.K. Jacobsen and R.C. Østergaard, DCB-specimen loaded with uneven bending moments, *International Journal of Fracture*, **141**, 2006, pp. 163–176 (doi: 10.1007/s10704-006-0071-x).

[2] ISO 15024:2001, Determination of mode I interlaminar fracture toughness, G_{Ic}, for unidirectionally reinforced materials, International Organization for Standardization, Geneva, 2001.

[3] S. Bennati, M. Colleluori, D. Corigliano and P.S. Valvo, An enhanced beam-theory model of the asymmetric double cantilever beam (ADCB) test for composite laminates, *Composites Science and Technology*, **69**, 2009, pp. 1735–1745. (doi: 10.1016/j.compscitech.2009.01.019).

[4] Q. Yang and B. Cox, Cohesive models for damage evolution in laminated composites, *International Journal of Fracture*, **133**, 2005, pp. 107–137. (doi: 10.1007/s10704-005-4729-6).

[5] B.F. Sørensen and T.K. Jacobsen, Characterizing delamination of fibre composites by mixed mode cohesive laws, *Composites Science and Technology*, **69**, 2009, pp. 445–456. (doi: 10.1016/j.compscitech.2008.11.025).

[6] B.F. Sørensen and S. Goutianos, Mixed Mode cohesive law with interface dilatation, *Mechanics of Materials*, **70**, 2014, pp. 76–93. (doi: 10.1016/j.mechmat.2013.11.006).

[7] R.M. Jones, *Mechanics of composite materials – 2nd ed.*, Taylor & Francis Inc., Philadelphia, 1999.

[8] J.R. Rice, A path independent integral and the approximate analysis of strain concentrations by notches and cracks, *Journal of Applied Mechanics*, **35**, 1968, pp. 379–386. (doi: 10.1115/1.3601206).

[9] P.S. Valvo and P. Cornetti, An energy equivalence approach for the estimation of the elastic interface constants for modelling delamination (in preparation).